Journal of Power Sources 196 (2011) 3350–3354

Contents lists available at ScienceDirect

Journal of Power Sources

journal homepage: www.elsevier.com/locate/jpowsour

Short communication

Improved capacitive properties of layered manganese dioxide grown as nanowires

O.A. Vargas, A. Caballero, L. Hernán*, J. Morales

Departamento de Química Inorgánica e Ingeniería Química, Universidad de Córdoba, Edificio Marie Curie, Campus de Rabanales, 14071 Córdoba, Spain

ARTICLE INFO

Article history:
Received 14 October 2010
Received in revised form 8 November 2010
Accepted 18 November 2010
Available online 25 November 2010

Keywords:
Birnessite
Naxmno2
Nanowire
Supercapacitor

ABSTRACT

Birnesite-type MnO_2 nanowires were prepared by direct reaction of $NaMnO_4$ with ethanol under hydrothermal conditions. Changing the pressure vessel load allowed a layered oxide in the form of nanoflakes to be obtained. The resulting nanowires were 10–20 nm wide and several micrometers long. Interestingly, the nanowires were poorly crystalline as revealed by their XRD patterns; also, they exhibited especially strong (1 0 0) reflections that were assigned to 1D growth of the particles. By contrast, the XRD pattern for the nanoflakes was consistent with an increased crystallinity as a result of 2D particle growth. The electrochemical properties of the nanowires and nanoflakes in 0.5 M Na_2SO_4 were evaluated by cyclic voltammetry and galvanostatic charge/discharge testing in two- and three-electrode cells. The nanowires exhibited an ideal capacitive behavior and a higher specific capacitance than the nanoflakes (191 vs. 157 F g^{-1}). In our opinion, the improved performance of the nanowires is a result of their high structural disorder and lattice strain rather than their higher specific surface area.

1. Introduction

The finding that RuO_2 exhibits a high pseudocapacitance (up to 700 F g^{-1} [1]) in aqueous electrolytes has boosted a search for alternative oxides based on transition metals less toxic and expensive than Ru. Although Fe and Mn are good candidates in this respect [2], the fact that Mn can occur in a greater number of oxidation states (particularly Mn^{3+} and Mn^{4+}) makes it the best choice [3]. A large number of papers dealing with the electrochemical properties of MnO_2 based compounds, both amorphous and crystalline, and deposited on carbon matrices, mainly as supercapacitors, have been published ([4,5] and references therein). The capacitance of birnessite, one of the forms of this oxide, barely exceeds 100 F g^{-1} in the pure compound [6,7]; this value is much lower than those for other crystalline forms such as hollandite [8]. In fact, α-MnO_2 in special morphologies such as hollow urchins and spheres [9], nanorods [10] or nanotubes [8] exhibits higher capacitance values. The improved electrochemical properties of these forms have been ascribed to either a mesoporous cluster structure [9] or a nanotubular microstructure and its large associated tunnel cavity [8]. The properties of the forms with special morphologies have also been investigated in birnessite-type MnO_2. The hierarchical hollow morphology obtained via a self-template synthetic route was found to increase capacitance—to an extent dependent on the particular sacrificial core (SiO_2 [11] or $MnCO_3$ [12]), however. In any case, this method is rather time-consuming and the accuracy of the hierarchical hollow manganese oxide nanospheres model requires further confirmation.

Layered MnO_2 nanowires have been found to exhibit stable cyclability and high capacity as a cathode material for rechargeable lithium batteries [13]. This special MnO_2 form precludes transformation into the spinel structure. As shown here, this peculiar morphology of layered MnO_2 also improves its performance as electrode material in supercapacitors. Following Ma et al. [13], the compound was prepared hydrothermally, but using different precursors and conditions in order to expedit its synthesis.

2. Experimental

2.1. Materials

The nanowires were synthesized by hydrothermal treatment of commercial $NaMnO_4$ (Aldrich) (1 g) disolved in an aqueous solution of 5 M NaOH (35 ml). The reductant was ethanol (3 ml). The resulting suspension was transferred to a Teflon-lined pressure vessel of 70 ml that was heated at 140 °C for 24 h and then allowed to cool to room temperature. Changing the load used allowed an appropriate particle shape to be obtained. The precipitate provided by the hydrothermal treatment was filtered, washed with deionized water and ethanol, and dried in the air at 80 °C for 24 h.

* Corresponding author. Tel.: +34 957 218620; fax: +34 957 218621.
E-mail address: iq1hepal@uco.es (L. Hernán).

0378-7753/$ – see front matter © 2010 Elsevier B.V. All rights reserved.
doi:10.1016/j.jpowsour.2010.11.097

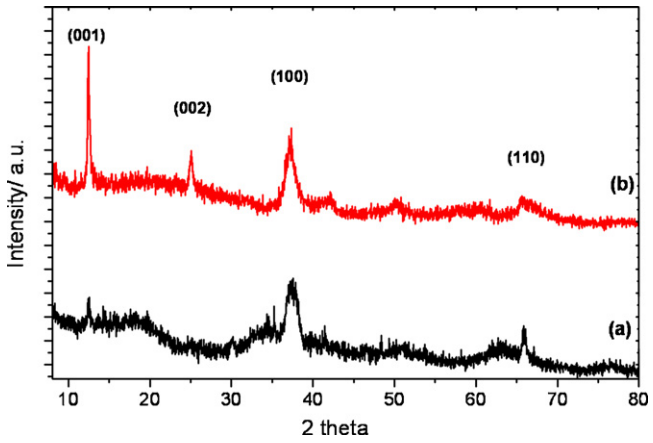

Fig. 1. XRD patterns for the products obtained in (a) a half-full pressure vessel and (b) 70% full pressure vessel.

2.2. Characterization of materials

XRD patterns were recorded on a Siemens D5000 X-ray diffractometer using non-monochromated Cu Kα radiation and a graphite monochromator for the diffracted beam. The scanning conditions for structural analysis were 15°–90° (2θ), a 0.03° step size and 12 s per step. Thermogravimetric measurements were made under ambient conditions, using a Setaram thermobalance (Setsys Evolution 16/18) at a heating rate of 10 °C min^{-1}. TEM images were obtained with a Jeol 2010 microscope operating at 200 keV and SEM images with a Jeol 6400 scanning electron microscope. Specific surface areas were determined with a Micromeritics ASAP 2020 instrument, using N_2 gas as adsorbate.

2.3. Electrochemical characterization

The electrodes were prepared by mixing the active material with carbon super P (Timcal), PVDF (Fluka) in a 80:10:10 weight ratio, slurrying with 1-methyl-2-pyrrolidinone (Sigma–Aldrich) on Ni foam (RECEMAT), drying at 80 °C for 1 h and pressing. Cyclic voltammetry tests were carried out on a Solartron 1286 instrument. Liquid cells were tested by using an aqueous solution of 0.5 M Na_2SO_4 (Sigma–Aldrich), Ni mesh and saturated calomel (SCE) as electrolyte, counter and reference electrodes, respectively. Swagelock-type two-electrode cells were tested under a potentiostatic regime and a galvanostatic regime, using a Solartron 1470 battery test unit. An amount of activated carbon (Norit DLC-S50) twice that of positive active material was used as negative electrode.

3. Results and discussion

3.1. Sample characterization

Fig. 1 shows the XRD pattern for the product obtained with a half-full pressure vessel. Its most salient feature was a high background and weak peaks typical of poorly crystalline phases. However, the pattern contained three well-defined peaks with spacings of 0.71, 0.24 and 0.14 nm that were assigned to the (0 0 1), (1 0 0) and (1 1 0) planes [13]. Worth special note is the intensity of the (1 0 0) plane—and, to a lesser extent, that of the (1 1 0) plane—, which was much higher than that of (0 0 1)—the strongest for a typical birnessite-type structure. This result was ascribed to a distinct habit growth of crystals that was apparent from the TEM images of Fig. 2a. Thus, particles exhibited marked 1D growth under the hydrothermal conditions used, that is, they tended to grow along

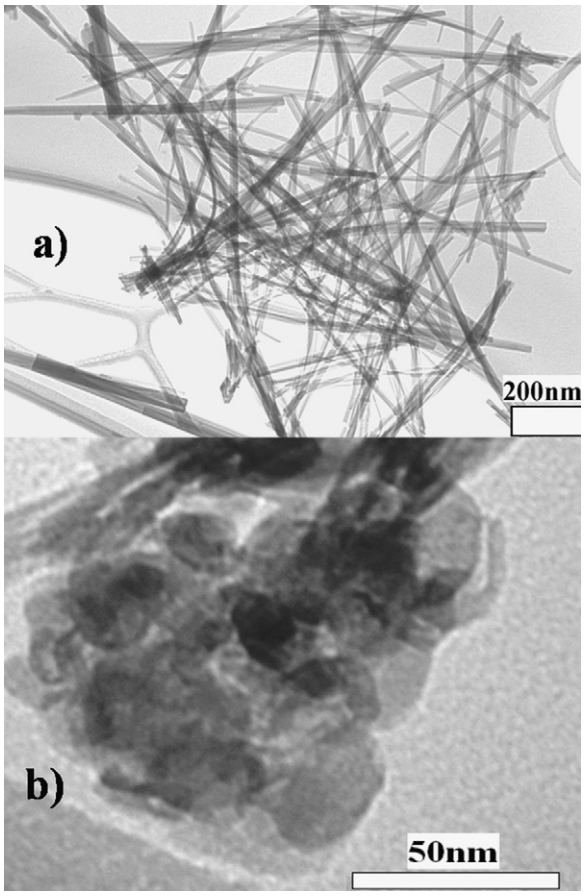

Fig. 2. TEM images for the products obtained in (a) a 50% full vessel and (b) a 70% full vessel.

(1 0 0), which resulted in an increased intensity in the (1 0 0) plane relative to the (0 0 1) plane. Therefore, the particles were nanowires 10–20 nm wide and several tens of a micrometer long. The energy dispersive spectra (EDS) for the samples confirmed the presence of Na in the structure and the quantitative analysis provided an estimated stoichiometry $Na_{0.23}MnO_2$. This sample will be henceforth referred to as "1D-birnessite".

A simple modification of the synthetic conditions (namely, loading the pressure vessel to 70% of its volume) had a marked effect on particle habit growth—and on the relative intensities of the diffraction peaks as a result. Thus, most particles adopted a flake-like morphology typical of a layered structure of the birnessite family (see Fig. 2b); also, their XRD pattern, Fig. 1b, was consistent with that previously reported for this layered compound, with strong peaks due to (0 0 l) reflections resulting from the flake-like particle morphology. The Na content was somewhat higher (the approximate stoichiometry was $Na_{0.31}MnO_2$). This sample was designated "2D-birnessite".

The previous samples exhibited two other differences worth noting. One was their thermal behavior. Thus, the TG curve for "2D-birnessite", Fig. 3a, exhibited three well-defined steps. The weight loss at low temperatures (below 400 °C) was assigned to hydration water, which was followed by the release of oxygen to form Mn_2O_3 (up to 700 °C) and, finally, of further oxygen to give the spinel Mn_3O_4. The total weight loss was 13.5%. By contrast, "1D-birnessite" exhibited a continuous weight loss, Fig. 3b, which precluded distinction of the weight losses due to water and oxygen. A similar behavior was previously observed by Devaraj and Munichandraiah [14] in a highly disordered birnessite the weight loss at 1000 °C of which was somewhat greater than that for our

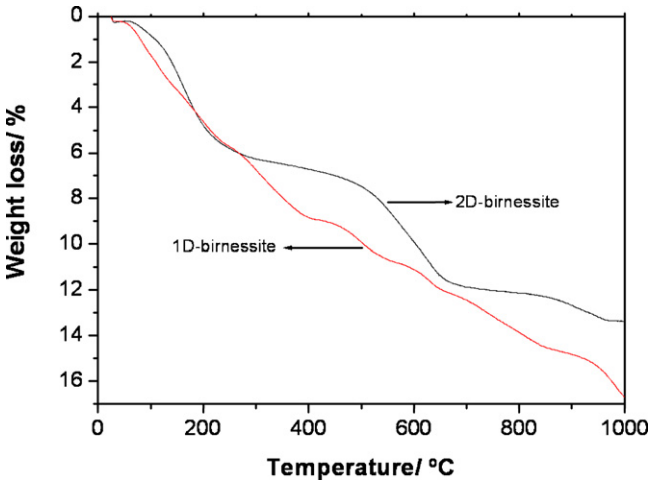

Fig. 3. TG curves for 1D- and 2D-birnessite.

sample (16.7%). In any case, reported losses for birnessite range from 23% [13] to 32% [14].

The second difference concerns textural properties. Fig. 4 shows the nitrogen adsorption/desorption isotherms for both samples. The isotherms were type IV and exhibited a small hystheresis loop in the higher-pressure region that was suggestive of a limited mesoporous system. The specific surface area of the nanowire particles, 76.3 $m^2\,g^{-1}$, was twice as high as that for the flake-like particles, 32.3 $m^2\,g^{-1}$. In order to analyse the pore structure of the as-prepared samples, their pore size distribution was evaluated by applying the BJH (Barret–Joyner–Halenda) method to the adsorption branch. As shown in the inset of Fig. 4, the adsorbed pore volume for "1D-birnessite" was higher than that for the "2D-birnessite". Also, the pore size distribution curve for "1D-birnessite" exhibited a peak at *ca.* 30 nm. Taking into account that the nanowire diameter was smaller than this value, the mesoporous system must have resulted from clustering of the voids between individual nanowires.

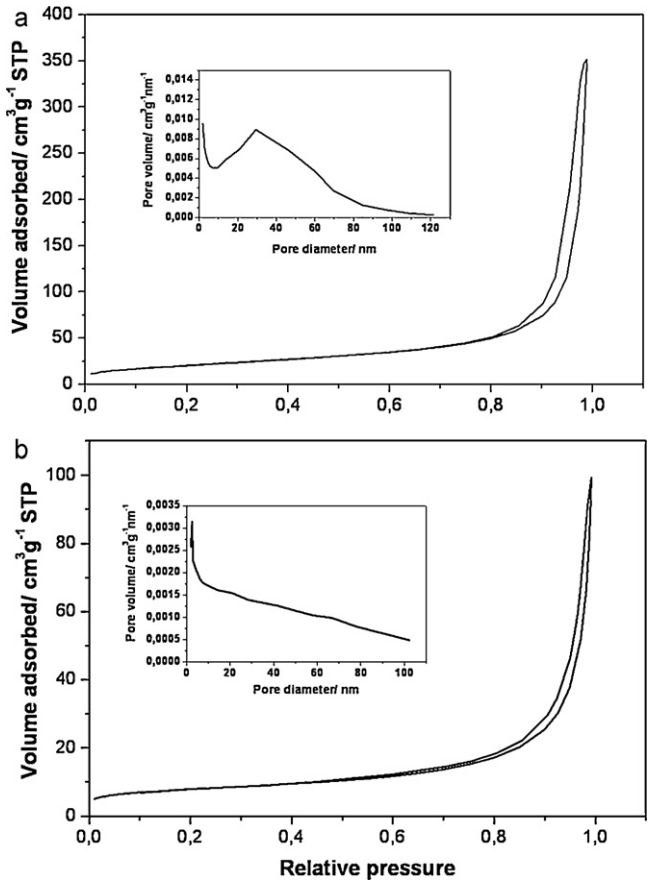

Fig. 4. N_2 adsorption/desorption isotherms for 1D-birnessite (a) and 2D-birnessite (b). Pore size distribution plots in both insets.

3.2. Electrochemical properties

The capacitive properties of the two samples were investigated by CV at a variable scan rate. The typical pseudorectangular shape of the curves for the electrode made from nanowire particles (Fig. 5) provides indirect evidence of its good reversibility. This indicates that the electrode is charged and discharged at a pseudoconstant rate throughout the voltammetric cycle, which is typical of a near-ideal capacitive behavior [9]. The specific capacitance values calculated from the CV curves are shown in Fig. 5b. The most salient feature of the curves is the high capacitance delivered by this peculiar birnessite-type geometry (191 $F\,g^{-1}$ at 1 $mV\,s^{-1}$, which considerably exceeds most reported values for this layered structure [6,7,11,15–18]). These birnessite samples usually have typical X-ray diffraction patterns similar to that of Fig. 1b and consist of polycrystalline grains. Capacitance values similar or even higher than ours have been reported for birnessite in special morphologies such as hierarchical hollow nanospheres [11], which are also highly structurally disordered as revealed by their XRD patterns. Moreover, the CV curves for this birnessite were rectangular in shape.

The CV curves for the electrode made from "2D-birnessite", Fig. 5c, were slightly differently shaped. As can be seen, they exhibited well-defined peaks due to intercalation/extraction of alkali cations present in the structure [19]. Also, this electrode delivered a lower specific capacitance and exhibited worse power capabilities than that made from nanobelt particles (see Fig. 5b). The higher specific surface area of the latter particles is no strong enough argument to justify their improved performance since birnessites of a higher surface area than nanobelt particles have been found to deliver lower specific capacitances [7]. The special habit of crystal growth involving rolling of the layers to adopt a nanowire morphology leads to a highly strained structure as revealed by the X-ray diffraction pattern, Fig. 1a, with a high background and weak, strongly broadened peaks. This high structural disorder was confirmed by high resolution electron microscopy (Fig. 6). Although the lattice was well-resolved, structural disorder was clearly apparent. The twisted layers hindered intercalation, which is otherwise detrimental to supercapacitor performance as a direct result of shrinkage and expansion in the lattice. In fact, one of the main reasons for the poorer capacitive properties of "2D-birnessite" must be the asymmetric, nonrectangular shape of its CV curve as a result of the extraction/insertion of Na ions. The highly strained nanoparticles may enhance surface adsorption and facilitate surface particle/electrolyte interactions via the following reaction:

$$(MnO_2)_{surface} + A^+ + e \leftrightarrow (MnO_2{}^-A^+)_{surface}$$

which provides an alternative to the intercalation mechanism used to explain the charge storage behavior of MnO_2 [3].

Additional information for the electrochemical behavior of these electrodes was obtained from asymmetric capacitors made from the birnessite-based compounds and activated carbon (AC). The specific capacitance at 5 $mV\,s^{-1}$ of a three-electrode cell made from the latter material was 64 $F\,g^{-1}$, which is somewhat lower than reported values for other activated carbons with higher specific surface areas [20]. Based on this result, and on that for the MnO_2

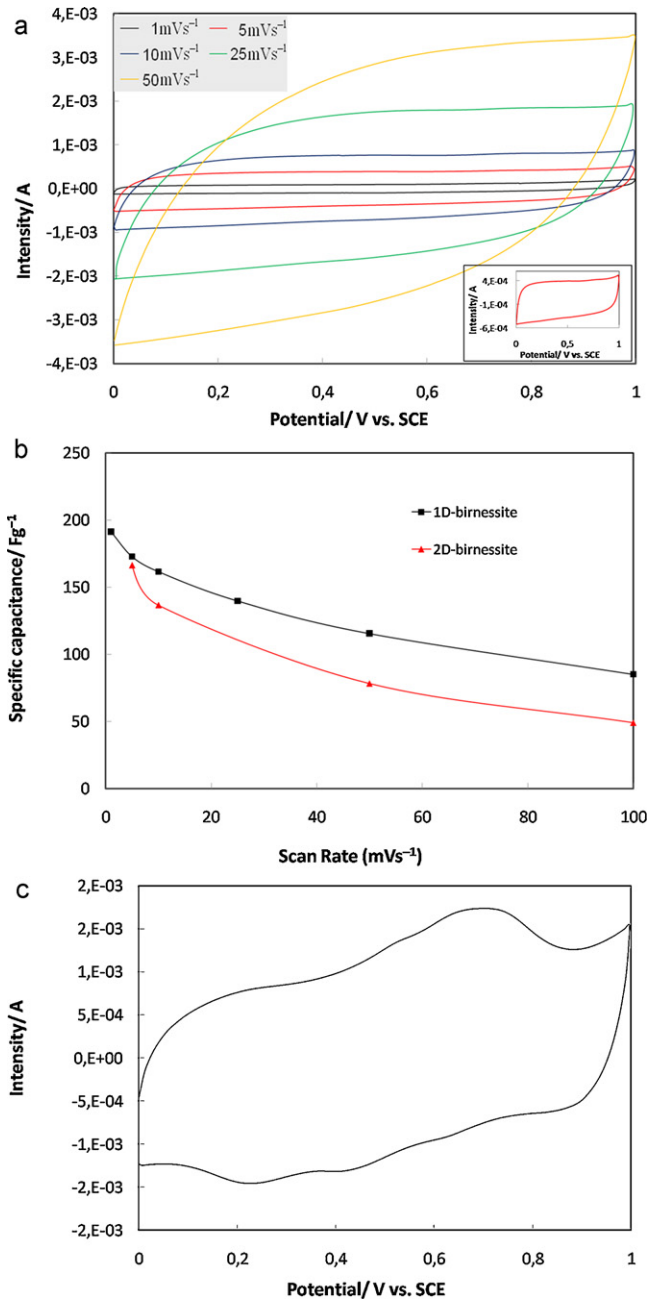

Fig. 5. (a) CV curves recorded at different scan rates (increasing rates from inside to outside in the main figure, 5 mV s^{-1} scan in the inset) for 1D-birnessite. (b) Specific capacitance values for both samples at different scan rates. (c) CV curve for 2D-birnessite as recorded at 5 mV s^{-1}.

electrode, the weight ratio of AC to birnessite was 2:1. Cycling tests on the asymmetric MnO_2/AC capacitors were carried out by adding Na_2HPO_4 to the electrolyte in order to improve capacity retention in the SC [16]. Again, all CV curves exhibited the typical rectangle-like shape (Fig. 7) irrespective of scan rate and number of cycles, which illustrates the capacitive behavior of the synthetic material. The specific capacitance of the capacitor was 24.4 F g^{-1} (based on the total mass of active electrode materials including the anode and cathode). This value is somewhat lower than those of other capacitors based on intercalation/deintercalation reactions (e.g., $NaMnO_2$/AC [20] and $Na_4Mn_9O_{18}$/AC [21,22], where Na ions are deintercalated and intercalated on charging and discharging the capacitor, respectively). In our case, the use of activated carbon

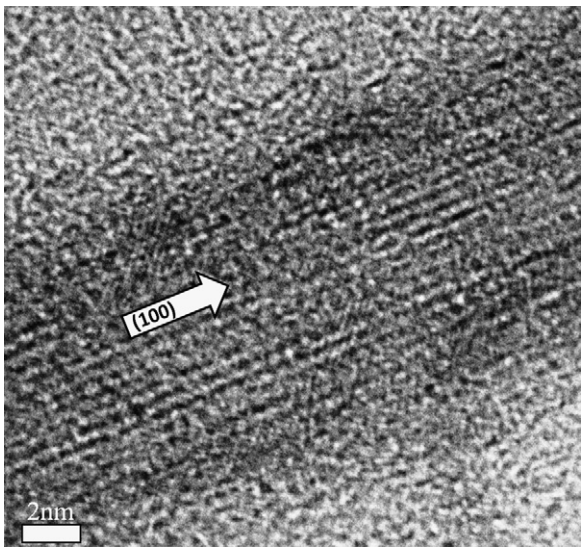

Fig. 6. HRTEM image of a 1D-birnessite particle. Arrow indicates the growth habit.

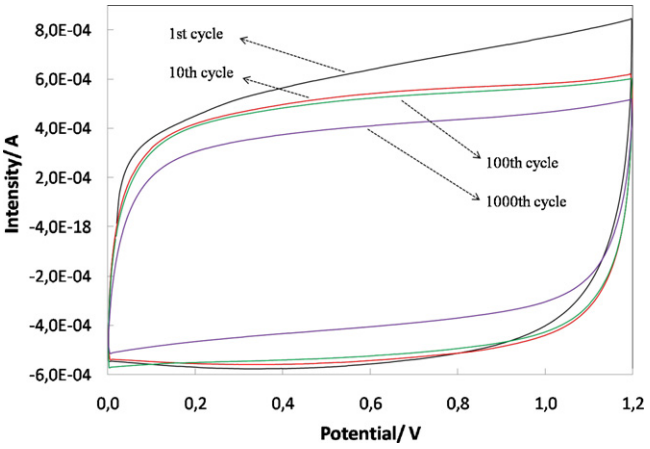

Fig. 7. CV curves for the MnO_2 (1D-birnessite)/AC capacitor. Na_2SO_4 0.5 M with additive of Na_2HPO_4 0.03 M as electrolyte. Scan rate: 5 mV s^{-1}.

of a lower capacitance precluded obtaining an increased specific capacitance from the capacitor.

We also used CV to examine the rate capabilities of the MnO_2/AC supercapacitor. This property was studied in a single cell by increasing the scan rate 5 mV s^{-1} every thousand cycles (see Fig. 8). The

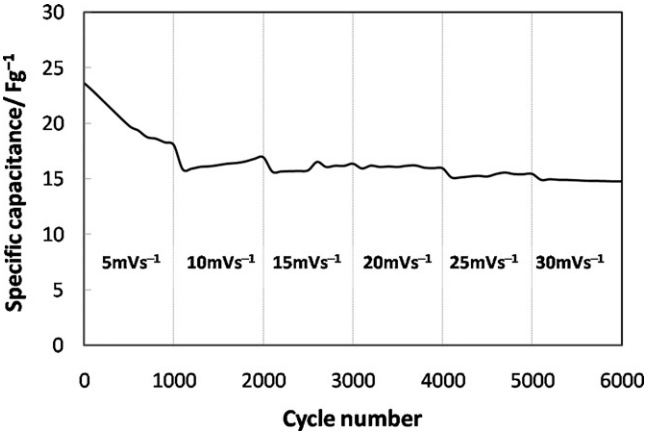

Fig. 8. Cycling behavior of 1D-birnessite towards increasing scan rates after every 1000 cycles. Values obtained from the CV curves.

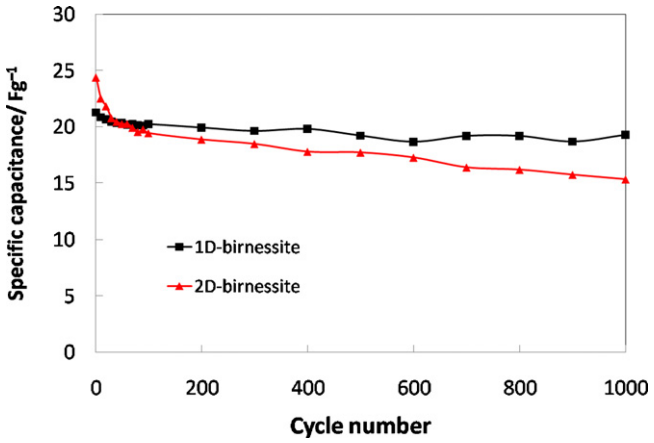

Fig. 9. Cycling behavior of both samples at a current density of 90 mA g^{-1} (based on total active mass of the birnessite and carbon electrodes). Values obtained in the galvanostatic tests.

greatest fall in specific capacitance was observed at 5 mV s^{-1}, with a tendency to stabilize around 18 F g^{-1} on prolonged cycling. At higher rates, the cell exhibited good capacity retention; thus, it retained 15 F g^{-1} at rates as high as 30 mV s^{-1}.

The improved electrochemical properties of the nanowire particles relative to the nanoflakes were also confirmed by their performance as electrodes in asymmetric capacitors. Fig. 9 shows the specific capacitance of the capacitors as a function of the number of cycles. Measurements were made under galvanostatic conditions, using a current density of 90 mA g^{-1} (based on the total active mass of the birnessite and carbon electrodes). Capacity retention was better for the supercapacitor made from "1D-birnessite" than for that made from "2D-birnessite". The specific capacitance delivered by the latter capacitor fell from 25 F g^{-1} to <15 F g^{-1} after a thousand of cycles. By contrast, the former capacitor retained its initial, somewhat lower capacitance (21 F g^{-1}) after a thousand cycles.

4. Conclusions

The capacitive properties of nanowire layered MnO_2 were studied and compared with those of nanoflake layered MnO_2, both of which were prepared hydrothermally. In addition to morphological differences, the nanowires exhibited a higher specific surface area and structural disorder than the nanoflakes. There were also differences in CV curve shape, as well as in delivered specific capacitance. Whereas the CV curves for the electrode made from nanowires were rectangular in shape and suggestive of an ideal capacitive behavior, those for the nanoflake electrode exhibited multiple peaks; this suggests that intercalation side reactions play some role in the electrochemical process. This has a detrimental effect on the electrode, which delivers a lower specific capacitance and exhibits degraded power capabilities as a result. The two compounds were also tested as electrode materials in asymmetric capacitors, using commercial activated carbon as negative electrode. Again, the nanowire capacitor performed better than the nanoflake capacitor. The higher specific surface area of the nanowires and, especially, the structural disorder needed to adopt this peculiar form, are the origin of their improved capacitive properties.

Acknowledgement

This work was performed with the financial support of the Ministerio de Ciencia e Innovación (Project MAT2008-03160) and Junta de Andalucía (Group FQM-175).

References

[1] J.P. Zheng, P.J. Cygan, T.R. Jow, J. Electrochem. Soc. 142 (1995) 2699.
[2] S.L. Kuo, N.L. Wu, Electrochem. Solid State Lett. 8 (2005) A495.
[3] H.Y. Lee, J.B. Goodenough, J. Solid State Chem. 144 (1999) 220.
[4] S. Chen, J. Zhu, X. Wu, Q. Han, X. Wang, ACS Nano 4 (2010) 2822.
[5] S.W. Lee, J. Kim, S. Chen, P.T. Hammond, Y.S. Horn, ACS Nano 4 (2010) 3889.
[6] D.J. Jones, E. Wortham, J. Rozière, F. Favier, J.L. Pascal, L. Manconduit, J. Phys. Chem. Solids 65 (2004) 235.
[7] T. Brousse, M. Toupin, R. Dugas, L. Athouël, O. Crosnier, D. Belanger, J. Electrochem. Soc. 153 (2006) A2171.
[8] W. Xiao, H. Xia, J.Y.H. Fuh, L. Lu, J. Power Sources 193 (2009) 935.
[9] M. Xu, L. Kong, W. Zhou, H. Lin, J. Phys. Chem. C 111 (2007) 19141.
[10] V. Subramanian, H. Zhu, R. Vajtai, P.M. Ajayan, B. Wei, J. Phys. Chem. B 109 (2005) 20207.
[11] X. Tang, Z.H. Liu, C.X. Zhang, Z. Yang, Z. Wang, J. Power Sources 193 (2009) 939.
[12] P. Yu, X. Zhang, Y. Chen, Y. Ma, Mater. Lett. 64 (2010) 1480.
[13] R. Ma, Y. Bando, L. Zhang, T. Sasaki, Adv. Mater. 16 (2004) 918.
[14] S. Devaraj, N. Munichandraiah, J. Phys. Chem. C 112 (2008) 4406.
[15] V. Subramanian, H. Zhu, B. Wei, J. Power Sources 159 (2006) 361.
[16] S. Komaba, A. Ogata, T. Tsuchikawa, Electrochem. Commun. 10 (2008) 1435.
[17] T. Bordjiba, D. Belanger, J. Electrochem. Soc. 156 (2009) A378.
[18] J. Yan, T. Wei, J. Cheng, Z. Fan, M. Zhang, Mat. Res. Bull. 45 (2010) 210.
[19] S.L. Kuo, N.L. Wu, J. Electrochem. Soc. 153 (2006) A1317.
[20] Q.T. Qu, Y. Shi, S. Tian, Y.H. Chen, Y.P. Wu, R. Holze, J. Power Sources 194 (2009) 1222.
[21] J.F. Whitacre, A. Tevar, S. Sharma, Electrochem. Commun. 12 (2010) 463.
[22] A.D. Tevar, J.F. Whitacre, J. Electrochem. Soc. 157 (2010) A870.